

# Neutrino Oscillation Results from MINOS and MiniBooNE

Tobias M. Raufer  
STFC Rutherford Appleton Laboratory, UK

After a brief introduction to neutrino oscillations and a review of the world knowledge of neutrino oscillation parameters, we introduce two current neutrino oscillation experiments, MINOS<sup>1</sup> and MiniBooNE<sup>2</sup>. MINOS makes precise measurements of the oscillation parameters  $|\Delta m_{32}^2|$  and  $\sin^2(2\theta_{23})$ . MiniBooNE tests neutrino oscillations in the parameter region reported by the LSND experiment, which would require a new neutrino state. We review recent experimental results from both experiments and give an outlook on future measurements.

## 1. Introduction

Neutrino oscillations are now a well established phenomenon. They follow from the non-zero and non-degenerate masses of the neutrino states and from the fact that mass and interaction eigenstates of the neutrino are not identical. The two sets of eigenstates are related by a unitary transformation, the PMNS matrix:

$$|\nu_\alpha\rangle = \sum_i U_{\alpha i}^* |\nu_i\rangle \quad (1)$$

Several experiments have observed neutrino oscillations and constrained the entries in the PMNS matrix, commonly parametrised by three rotation angles  $\theta_{ij}$  and a complex phase  $\delta$ . The Super-Kamiokande (SuperK) experiment in Japan measured the disappearance of neutrinos produced in the upper atmosphere dependent on neutrino flavor, energy and zenith angle [1], pointing to the characteristic  $L/E$  signature of neutrino oscillations. The K2K experiment confirmed this result [2] using an accelerator neutrino beam measured at a distance of 250 km. Neutrino oscillations have also been measured in solar neutrinos. After a long list of experiments starting as early as the 1960s, the most precise measurements of solar neutrino oscillations comes from the Sudbury Neutrino Observatory (SNO) [3]. Finally, measurements at nuclear reactors have established the smallness of the third mixing angle,  $\theta_{13}$ . The best limit on this parameter comes from the CHOOZ [4] experiment in France.

The world knowledge on neutrino oscillation parameters from a global fit to all available experimental data is shown in Table I (taken from [5]). The final column shows the experiment with the biggest contribution to a given parameter. It is clear from this table that neutrino physics has entered the realm of precision measurements.

Table I Global fit neutrino oscillation parameters

Parameter	Best fit $\pm 1\sigma$	Experiment
$\Delta m_{21}^2$	$(7.6 \pm 0.2) \times 10^{-5} \text{eV}^2$	KamLAND
$\sin^2 \theta_{12}$	$0.320 \pm 0.023$	SNO
$ \Delta m_{32}^2 $	$(2.4 \pm 0.15) \times 10^{-3} \text{eV}^2$	MINOS
$\sin^2(2\theta_{23})$	$0.50 \pm 0.063$	SK atm
$\sin^2 \theta_{13}$	$< 0.05 \text{ at } 3\sigma$	CHOOZ

### 1.1. Sterile Neutrinos

The number of active neutrinos, measured by the LEP experiments using the width of the  $Z^0$  resonance [6], is consistent with three at high precision. There is however no limit on the number of non-interacting neutrinos, customarily called sterile neutrinos.

One motivation for the search for sterile neutrinos is a result by the LSND experiment [7] which claimed evidence for  $\bar{\nu}_\mu \rightarrow \bar{\nu}_e$  oscillations with a mass splitting incompatible with the experimental results given in the previous section.

The MiniBooNE experiment was designed specifically to test this so-called “LSND anomaly”.

MINOS also investigates sterile neutrino models by measuring neutral current neutrino interactions.

## 2. The MINOS experiment

MINOS is a long-baseline neutrino oscillation experiment at Fermilab’s “Neutrinos at the Main Injector” (NuMI) beam line. It utilises two detectors situated at distances of  $\sim 1$  km and  $\sim 735$  km from the neutrino production target respectively. The near detector measures the beam composition and energy spectrum, making use of the large number of neutrino interactions close to the source. This is compared to the measurement at the far detector in order to study neutrino oscillations.

<sup>1</sup>MINOS: Main Injector Neutrino Oscillation Search

<sup>2</sup>BooNE: Booster Neutrino Experiment

## 2.1. The NuMI beam

The NuMI beam line uses 120 GeV protons from the Main Injector accelerator incident on a segmented graphite target where they produce mainly  $\pi^-$ - and  $K^-$ -mesons. These secondary particles are focused by two parabolic horns and subsequently decay in a 675 m long helium-filled decay volume to produce neutrinos. The remaining hadrons are absorbed in a water-cooled beam dump at the end of the decay volume while muons produced in the decay are absorbed in the rock separating the near detector hall from the hadron absorber. A small fraction of muons further decay before being absorbed, producing electron and anti-muon neutrinos. The resulting neutrino beam has the following composition: 92.9%  $\nu_\mu$ , 5.8%  $\bar{\nu}_\mu$ , 1.2%  $\nu_e$  and 0.1%  $\bar{\nu}_e$  for the low energy (LE) beam configuration.

The focusing peak and thus the neutrino energy spectrum of the NuMI beam can be varied by moving the target with respect to the magnetic horns. This feature is unique to the NuMI beam and is used in all MINOS analyses in order to reduce systematic uncertainties related to hadron production in the neutrino production target.

## 2.2. The MINOS detectors

The MINOS detectors are functionally identical steel/scintillator sampling calorimeters equipped with a magnetic field to allow charge sign determination of muon tracks. The far detector has a mass of 5.4 kt and is situated at a depth of 2130 m.w.e. in the Soudan Underground Laboratory. The smaller near detector is  $\sim 1$  kt and is situated 100 m below ground at Fermilab. The detectors are constructed from 2.5 cm thick steel planes mounted with a 1 cm thick layer of plastic scintillator segmented into  $\sim 4$  cm wide strips. The scintillation light is collected by wavelength shifting fibres and readout by multi-anode photomultiplier tubes.

The detectors are calibrated using single particle response data collected with a smaller 12 t calibration detector at the CERN PS test-beam and a light injection system tracking PMT gain variations. Inter-detector calibration of the energy response is achieved using cosmic ray muons.

## 3. MINOS data analysis

In this document, we present results from two different analyses and give a status report on a third one. They can be classified by the main type of interaction of interest:  $\nu_\mu$  charged current, neutral current and  $\nu_e$  charged current. At the time of writing of this document, MINOS has collected an integrated  $4.8 \times 10^{20}$  protons-on-target (POT), most of which was recorded

in the LE beam configuration. The results reported here use a data sample of  $2.5 \times 10^{20}$  POT.

The three analyses have many steps in common. Firstly, they all rely on a good understanding of the details of the neutrino beam. The major unknown here is the production of hadrons in the NuMI target. A detailed Monte Carlo simulation of the beam line components based on Fluka05 reproduces the data well but not perfectly. To further improve data/Monte Carlo agreement, the hadron production is parametrised as a function of  $x_F$  and  $p_t$  and a simultaneous fit is performed to the near detector spectra in various different beam configurations. Individual neutrino interactions are reweighted according to the  $x_F$  and  $p_T$  of the parent pion (or kaon). Figure 1 shows near detector data and Monte Carlo for two different beam configurations before and after the tuning procedure. A total of seven different beam configurations

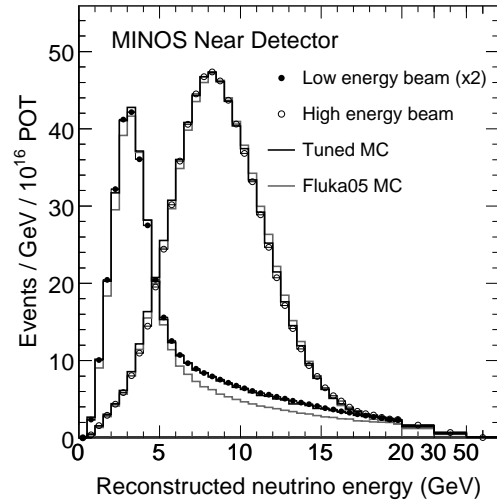


Figure 1: Near Detector data and Monte Carlo for the low and high energy beam configurations. The grey lines show the untuned Monte Carlo simulation based on Fluka05. The black lines show the Monte Carlo after hadron production tuning is applied. The agreement is much improved.

were used in the fit. The thus improved hadron production model is then used in the prediction of the far detector neutrino energy spectrum.

Another common feature is the “blind analysis” technique. This involves not looking at the far detector data until the complete analysis procedure – e.g. selection cuts, extrapolation, fitting, etc. – is defined. The near detector data is not sensitive to oscillations at the atmospheric scale and was therefore accessible throughout the development of the analyses, thus allowing to understand low level detector effects in the data.

### 3.1. $\nu_\mu$ charged current analysis

The charged current disappearance analysis is the main analysis of MINOS. Measuring the charged current energy spectrum in both detectors, MINOS measures the neutrino oscillation parameters  $|\Delta m_{32}^2|$  and  $\sin^2(2\theta_{23})$ . The analysis reported here is an update of our initial results published in [8].

Charged current candidate events are selected by demanding a reconstructed track within  $53^\circ$  of the beam direction with a vertex inside the fiducial volume and in time with the beam spill. To further reject neutral current background events a likelihood-ratio discriminant is constructed from six variables, reflecting event topology, energy loss, inelasticity, etc. A more detailed discussion of the charged current event selection and extrapolation to the far detector for this analysis can be found in [9].

Figure 2 shows the selected charged current energy spectrum corresponding to an exposure of  $2.5 \times 10^{20}$  POT. The points with error bars show the far detector data and the black and red lines show unoscillated and oscillated Monte Carlo predictions respectively. The best-fit values for the oscillation

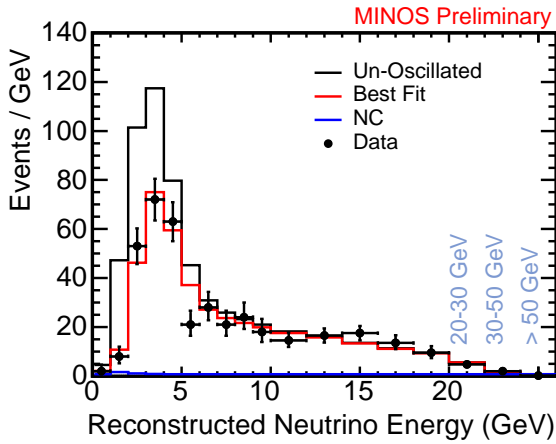


Figure 2: Reconstructed far detector neutrino energy spectrum. The black markers with error bars show the data, the black and red lines show unoscillated and best-fit Monte Carlo predictions. The neutral current background is shown in blue.

parameters are:  $|\Delta m_{32}^2| = 2.38^{+0.20}_{-0.16} \times 10^{-3} \text{eV}^2$  and  $\sin^2(2\theta_{23}) = 1.00_{-0.08}$ . The errors given combine both statistical and systematic errors. The latter were included in the fit via nuisance parameters.

### 3.2. Neutral current analysis

If neutrino oscillations only involve the usual active neutrino flavours, the neutral current event rate remains unchanged. The measurement of neutral current interactions therefore allows the investigation of

oscillations into sterile neutrinos, i.e. neutrino states with no standard model interactions.

Neutral current events in MINOS are selected with a set of simple cuts using event shape variables. The main distinguishing feature between charged current and neutral current events is the presence or lack of a muon in the final state leading to a reconstructed track in the detector. Short events, events with no track and events where the reconstructed track is shorter than the hadronic shower are classified as neutral current.

In the near detector, additional cuts on spacial separation and timing are applied to make sure the event is well reconstructed and not a remnant of another bigger event in the vicinity.

In the far detector, an additional set of cuts removing cosmic rays and low energy noise is applied. The resulting neutral current reconstructed energy spectrum is shown in Figure 3.

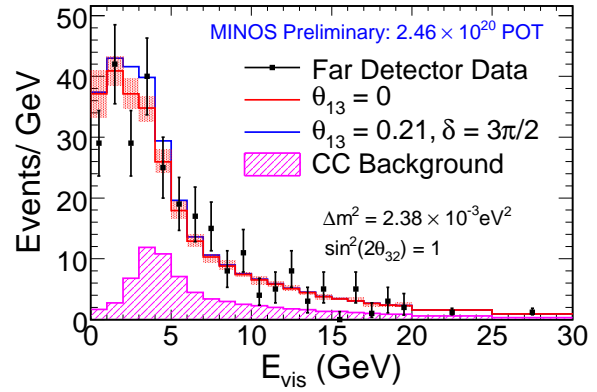


Figure 3: Far Detector reconstructed energy spectrum for selected neutral current events. The data is shown as black points with error bars, the Monte Carlo is shown in blue and red for two extremes of the third angle  $\theta_{13}$ . The charged current background is shown in pink.

The Monte Carlo expectation for this spectrum depends on the value of the third mixing angle  $\theta_{13}$  since  $\nu_e$  interactions have a high probability of being classified as neutral currents in this analysis. We therefore show two Monte Carlo lines, one for  $\theta_{13} = 0$  (red) and one for electron neutrino appearance at the CHOOZ limit (blue). The width of the red band reflects the systematic uncertainties. For reconstructed energies below 3 GeV, a deficit with respect to the Monte Carlo expectation for  $\theta_{13} = 0$  of  $1.15\sigma$  is observed. The data is thus consistent with no active neutrino disappearance.

While the above discussion is model independent, it is also instructive to compare the data to a particular model involving mixing between active and sterile neutrinos. We use a simple model introducing a single sterile neutrino state and retaining one-mass-scale dominance. Assuming no mixing of the first and sec-

ond mass eigenstates with the sterile state and assuming that the first and fourth mass eigenstate are nearly degenerate leads to the following oscillation probabilities:

$$\begin{aligned} P_{\nu_\mu \rightarrow \nu_\mu} &= 1 - 4|U_{\mu 3}|^2(1 - |U_{\mu 3}|^2) \sin^2(1.27 \Delta m_{32}^2 L/E) \\ P_{\nu_\mu \rightarrow \nu_e} &= 4|U_{\mu 3}|^2|U_{e 3}|^2 \sin^2(1.27 \Delta m_{32}^2 L/E) \\ P_{\nu_\mu \rightarrow \nu_s} &= 4|U_{\mu 3}|^2|U_{s 3}|^2 \sin^2(1.27 \Delta m_{32}^2 L/E) \\ P_{\nu_\mu \rightarrow \nu_\tau} &= 1 - P_{\nu_\mu \rightarrow \nu_\mu} - P_{\nu_\mu \rightarrow \nu_e} - P_{\nu_\mu \rightarrow \nu_s}. \end{aligned} \quad (2)$$

The charged and neutral current energy spectra are fitted simultaneously to this 4-flavour model under two different scenarios. The first scenario assumes no  $\nu_e$  appearance, i.e.  $|U_{e 3}|^2 = 0$ , the second assumes  $\nu_e$  appearance at the CHOOZ limit,  $|U_{e 3}|^2 = 0.04$ . The results are:

$$\begin{aligned} |U_{s 3}|^2 &= 0.14^{+0.18}_{-0.13} \quad |U_{\mu 3}|^2 = 0.50^{+0.16}_{-0.15} \quad (|U_{e 3}|^2 = 0) \\ |U_{s 3}|^2 &= 0.21^{+0.20}_{-0.12} \quad |U_{\mu 3}|^2 = 0.48^{+0.18}_{-0.12} \quad (|U_{e 3}|^2 = 0.04) \end{aligned}$$

Systematic errors were included in the fit as nuisance parameters; the errors quoted above thus include both statistical and systematic uncertainties. The values for  $|U_{\mu 3}|^2$  are consistent with the parameter  $\sin^2(2\theta_{23})$  reported in section 3.1.

More details on the analysis of neutral current interactions in MINOS can be found in [10].

### 3.3. $\nu_e$ appearance analysis

The  $\nu_e$  appearance analysis investigates the subdominant oscillation channel  $\nu_\mu \rightarrow \nu_e$  which is sensitive to the third angle in the PMNS matrix,  $\theta_{13}$ . The non-observation of the reverse process at the CHOOZ reactor experiment [4] provides an upper limit for this parameter. A potential observation of  $\nu_e$  events in the MINOS far detector beyond the inherent level in the NuMI beam would provide evidence for a non-zero value below the CHOOZ limit.

$\nu_e$  events are characterised by an electromagnetic shower in the detector in addition to the hadronic activity caused by the struck nucleus. The success of this analysis therefore relies on the ability to identify electromagnetic showers in a large background of hadronic activity. Due to the relatively coarse segmentation of the MINOS detectors, this is a very difficult task.

$\nu_e$  candidates are selected using a neural network technique. Since these techniques rely on good data/Monte Carlo agreement, two independent data driven methods using the near detector have been developed in order to improve the modeling of the backgrounds. This is possible since the baseline at the near detector is too short for oscillations to develop.

One method takes well understood, well reconstructed charged current events and removes the muon track, leaving a sole hadronic shower. This remnant

event is then reconstructed again in order to determine, how often such an event is misclassified as an electromagnetic shower. Using this method, a discrepancy of 20% is found, with the Monte Carlo overestimating the background. A second method compares data taken with and without the focusing horns being powered. This allows a deconvolution of the different background components since the composition is quite different in the two samples.

The results obtained using the two different methods are consistent, justifying an ad-hoc correction which is applied to the Monte Carlo prediction. The background estimates are extrapolated to the far detector where the sensitivity to measuring  $\theta_{13}$  is evaluated. These sensitivities for three different exposures are shown in Figure 4.

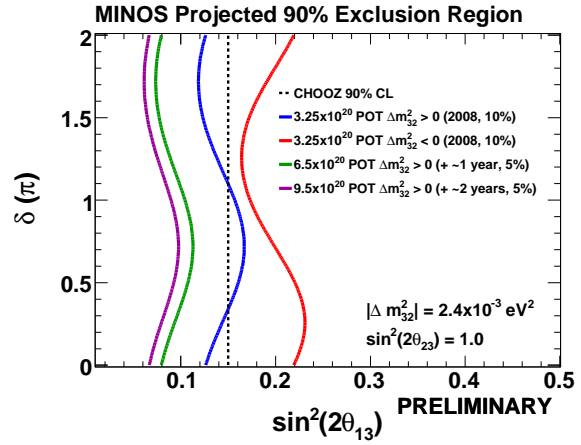


Figure 4: Sensitivity to  $\theta_{13}$  for three different exposures. For our current data set of  $3.25 \times 10^{20}$  the sensitivity for both the normal (blue) and inverted (red) mass hierarchies are shown. A 10% systematic error is included in all predictions. With increasing statistics, improvements over the CHOOZ bound can be made.

The data for this analysis are still blinded and final studies are being performed, including the investigation of data “sidebands”. Results from this analysis are eagerly awaited and are expected later this year.

## 4. The MiniBooNE experiment

MiniBooNE is a short-baseline neutrino oscillation experiment using Fermilab’s booster neutrino beam line. With a source-detector distance of  $\sim 0.5$  km and a peak neutrino energy of 0.8 GeV it is specifically designed to test the parameter space of the LSND claim discussed in section 1.1.

MiniBooNE uses a conventional neutrino beam similar to the NuMI beam described above. The booster’s 8 GeV protons impinge on a beryllium target at a rate of up to 4 Hz. The secondary mesons are focused by

a single pulsed magnetic focusing horn and allowed to decay in a 50 m-long decay region. The detector is separated from the end of the decay volume by  $\sim 500$  m of earth.

The MiniBooNE detector consists of a spherical volume filled with 800 tons of mineral oil ( $\text{CH}_2$ ), acting both as a scintillator and Cerenkov medium. The light produced in the detector is read out by 1280 inward facing 8-inch photomultiplier tubes (PMTs) providing a 10% photo-cathode coverage, viewing a target volume 575 cm in diameter. The target volume is surrounded by a 35 cm thick, optically isolated veto region viewed by 240 PMTs.

## 5. MiniBooNE oscillation analysis

The MiniBooNE analysis was conducted in a blinded fashion. Only Monte Carlo simulation and data insensitive to  $\nu_\mu \rightarrow \nu_e$  oscillations was used to develop the analysis procedure.

As in the MINOS experiment, hadron production uncertainties in the target are an important contributor to the systematic error for MiniBooNE analyses. MiniBooNE uses a Sanford-Wang parametrisation to the pion data from the HARP experiment [11] and a fit to the world kaon production data in the range of 10–24 GeV to improve on this uncertainty. The quoted uncertainties are 17% for the pion and 30% for the kaon flux. The predicted kaon flux is checked using off-axis muon counters and high energy events in the MiniBooNE detector.

To select electron-like neutrino interactions in MiniBooNE, events are first divided into so-called subevents, i.e. sets of PMT hits which are clustered within  $\sim 100$  ns. Only subevents in time with the beam spill are selected. Subevents are required to have more than 200 hits in the tank, less than 6 hits in the veto region and a reconstructed vertex position with  $R < 500$  cm, eliminating cosmic ray muons and associated decay electrons.  $\nu_e$  charged current event candidates are required to have exactly one subevent.

After these initial selection cuts, two visible energy dependent likelihood ratio discriminants are constructed in order to further reduce the backgrounds. The first one separates muon-like from electron-like Cerenkov rings. The second discriminant separates the remaining events into electron-like events and events from  $\pi^0$ -decay. For the complete selection, the Monte Carlo predicts an efficiency for  $\nu_e$  charged current quasi-elastic events of  $20.3 \pm 0.9\%$ . Further details on the event selection can be found in [12].

The MiniBooNE collaboration decided to open their blinded data set in stages, revealing more and more details about the data while still blind to the oscillation result. During this unblinding procedure, it was found that data and Monte Carlo expectation resulted in a bad  $\chi^2$  for both the oscillation and null

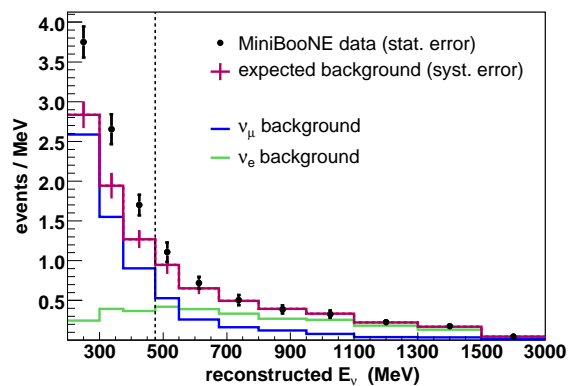


Figure 5: Reconstructed neutrino energy spectrum from MiniBooNE for data (black dots) and Monte Carlo (magenta line). The data is shown with statistical error bars and the Monte Carlo shows the expected non-oscillation background including systematic errors. A low energy threshold of 475 MeV was applied to the analysis.

hypothesis. The disagreement was found to come from the lowest energy events. It was therefore decided to move the energy threshold for the analysis to 475 MeV, while still showing the lower energy events to the public. The resulting visible energy spectrum for data and Monte Carlo is shown in Figure 5.

Above the energy threshold, the data does not show a significant excess and is consistent with no electron-neutrino appearance at the  $1 \text{ eV}^2$  scale. MiniBooNE is therefore able to exclude a region in the  $\Delta m^2 - \sin^2 2\theta$  parameter space. Figure 6 shows how the MiniBooNE result compares with previous experiments Bugey, KARMEN and LSND. It can be seen that MiniBooNE rules out large parts of the LSND favoured region (shown in blue). Assuming that neutrinos and antineutrinos oscillate in the same way and using a two-neutrino approximation, LSND and MiniBooNE are incompatible at 98% C.L.

Several potential sources for the reported excess of events below the 474 MeV threshold have been discussed and are currently being investigated by the collaboration. At the time of writing, no new results on this issue were available.

## 6. Summary

Neutrino oscillations have been introduced and evidence and current world knowledge on oscillation parameters from several experiments have been reported. We reported the latest neutrino oscillation results from the MINOS and MiniBooNE experiments, detailing aspects of the MINOS  $\nu_\mu$  charged current, neutral current and  $\nu_e$  appearance analysis as well as the MiniBooNE two-flavour oscillation analysis.

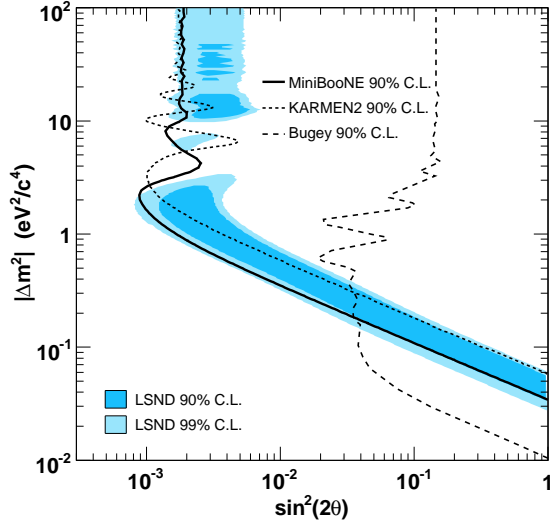


Figure 6: The MiniBooNE 90% exclusion curve is shown as a solid black line along with the curves from the KARMEN and Bugey experiments (dashed). The LSND allowed regions are shown in blue. MiniBooNE and LSND are incompatible at 98% C.L.

## Acknowledgments

The MINOS work reported here was supported by the US DOE; the UK STFC; the US NSF; the State and University of Minnesota; the University of Athens, Greece and Brazil's FAPESP and CNPq. MINOS would like to thank the Minnesota Department of Natural Resources, the crew of the Soudan Underground Laboratory, and the staff of Fermilab for their contributions to this effort.

The author would like to thank the MiniBooNE collaboration and Rustem Ospanov for the material provided. Furthermore, we would like to thank the organisers of FPCP08 for the help provided.

## References

- [1] Y. Ashie *et al.* [Super-Kamiokande Collaboration], Phys. Rev. D **71** 112005 (2005).
- [2] M. H. Ahn *et al.* [K2K Collaboration], Phys. Rev. D **74** 072003 (2006).
- [3] Q. R. Ahmad *et al.* [SNO Collaboration], Phys. Rev. Lett. **89**, 011301 (2002)
- [4] M. Apollonio *et al.* [CHOOZ Collaboration], Eur. Phys. J. C **27**, 331 (2003)
- [5] M. Maltoni, T. Schwetz, M. A. Tortola and J. W. F. Valle, arXiv:hep-ph/0405172v6.
- [6] ALEPH Collaboration and DELPHI Collaboration and L3 Collaboration and OPAL Collaboration, Phys. Rept. **427**, 257 (2006)
- [7] A. Aguilar *et al.* [LSND Collaboration], Phys. Rev. D **64**, 112007 (2001)
- [8] D. G. Michael *et al.* [MINOS Collaboration], Phys. Rev. Lett. **97**, 191801 (2006)
- [9] P. Adamson *et al.* [MINOS Collaboration], arXiv:0708.1495 [hep-ex].
- [10] P. Adamson *et al.* [MINOS Collaboration], arXiv:0807.2424 [hep-ex].
- [11] M. G. Catanesi *et al.* [HARP Collaboration], Nucl. Phys. B **732**, 1 (2006)
- [12] A. A. Aguilar-Arevalo *et al.* [The MiniBooNE Collaboration], Phys. Rev. Lett. **98**, 231801 (2007)